Fall 2023

Growth and Characterization of SM3HFBI5

Patrick Lambdin
Missouri State University, pl837s@MissouriState.edu

Recommended Citation
Lambdin, Patrick, "Growth and Characterization of SM3HFBI5" (2023). *MSU Graduate Theses*. 3912.
https://bearworks.missouristate.edu/theses/3912

GROWTH AND CHARACTERIZATION OF SM$_3$HFBI$_5$

A Master's Thesis

Presented to

The Graduate College of

Missouri State University

In Partial Fulfillment

Of the Requirements for the Degree

Master of Science, Materials Science

By

Patrick Lambdin

December 2023

GROWTH AND CHARACTERIZATION OF SM_3HFBI_5

Materials Science

Missouri State University, December 2023

Master of Science

Patrick Lambdin

ABSTRACT

First found experimentally in 2015, topological Weyl materials are desirable compounds that have garnered much interest due to their ability to conduct electricity via their surface states even though the bulk material is a semimetal. Such a candidate, Sm_3HfBi_5, was discovered with a flux crystal growth method, following an extensive amount of reaction syntheses. This thesis reports on the discovery, growth, structural characterization via x-ray diffraction, and magnetization measurements on Sm_3HfBi_5.

KEYWORDS: topological material, flux growth, Weyl semimetal, single crystal

GROWTH AND CHARACTERIZATION OF SM_3HFBI_5

By

Patrick Lambdin

A Master's Thesis
Submitted to the Graduate College
Of Missouri State University
In Partial Fulfillment of the Requirements
For the Degree of Master of Scienc, Materials Science

December 2023

Approved:

Tiglet Besara, Ph. D., Thesis Committee Chair

Kartik Ghosh, Ph. D., Committee Member

Robert Mayanovic, Ph. D., Committee Member

Julie Masterson, Ph. D., Associate Provost and Dean of the Graduate College

ACKNOWLEDGEMENTS

First and foremost, thank you to my wife, Dr. Kristin Harper, for encouraging me to return to school and supporting me throughout many late nights, failed tests, and periods of self-doubt. Secondly, thank you to Dr. Tiglet Besara for his continuous support securing grants, advising me through undergraduate as well as graduate degrees, and for talking me into switching to a physics major in the first place. Thirdly, thank you to several students who in particular helped me survive the grind of graduate school, namely: Sarah Longworth, Md. Fahel Bin Noor, and Nusrat Yasmin.

Thank you also to the other unnamed students and faculty members who helped me in untold ways in my time at Missouri State whether it were in office hours, help with homework, or in securing internships during both the school year and the summer months.

Nisi finitum nihil satis est.

I dedicate this thesis to Kristin, for supporting me enough to complete it, and to my immediate family, Curt, Peggy, Katie, Spencer, and Hannah for nurturing a desire for lifelong learning.

TABLE OF CONTENTS

Introduction Page 1

Methods Page 5
  Flux Growth Page 5
  Reactions Page 13
  Experimental Reaction Phase Page 13
  Focused Reaction Sets Page 15

Results Page 18
  Exploratory Reaction Results Page 18
  Focused Reaction Results Page 19
  Single Crystal X-ray Diffraction Page 20
  Magnetic Characteristics Page 25

Conclusion Page 33

References Page 34

LIST OF TABLES

Table 2.1. First sets of experimental reactions Page 14

Table 2.2 Second sets of experimental reactions Page 15

Table 2.3 Sets of focused reactions Page 17

Table 3.1 Single crystal X-ray diffraction data and parameters Page 23

Table 3.2 Atomic coordinates, and equivalent displacement parameters Page 23

LIST OF FIGURES

Figure 1.1. Historical timeline of the field of topological semimetals Page 1

Figure 1.2 Variations on spin orbit coupling Page 2

Figure 2.1. Thermodynamics of crystal growth Page 6

Figure 2.2 Crystal growth techniques Page 7

Figure 2.3 A set of alumina crucibles used for reactions Page 8

Figure 2.4 The glovebox and Schlenk line Page 9

Figure 2.5 A fully sealed reaction ready for the furnace. Page 11

Figure 3.1 Images of grown crystals Page 19

Figure 3.2 Sm_3HfBi_5 crystals Page 20

Figure 3.3 Sm_3HfBi_5 after only a few hours air exposure Page 20

Figure 3.4 "Powder" x-ray diffraction pattern Page 21

Figure 3.5 Looking down the length of the c-axis Page 24

Figure 3.6 The unit cell of Sm_3HfBi_5 Page 24

Figure 3.7 Magnetic susceptibility of Sm_3HfBi_5 Page 25

Figure 3.8 Magnetic susceptibility and resistivity values of La_3HfBi_5 Page 28

Figure 3.9 Magnetic susceptibility of Sm_3TiSb_5 Page 29

Figure 3.10 Magnetic susceptibility of Sm_3ZrBi_5 Page 30

Figure 3.11 Sm-Sm bonds running down the length of Sm_3HfBi_5 Page 31

Figure 3.12 Magnetization in an external magnetic field for Sm_3HfBi_5 Page 32

INTRODUCTION

This project began as an effort to grow novel topological materials in my undergraduate career at Missouri State University, with the original, stated goal of finding new ternary materials, or materials composed of three elements. Toward the end of discovering any new material, dozens of flux crystal growth reactions have been completed. In that time, one compound, Sm_3HfBi_5, has proven itself especially worthy of further characterization both for its limited discussion in scientific literature and its possible membership in that exclusive collection of materials known as Weyl semimetals. Figure 1.1 shows the developmental history and some band structures of Weyl semimetals.

Weyl semimetals are an area of recent interest in condensed matter physics and are defined by having electron energy bands which narrowly intersect at a point called a Weyl node [1-2]. The presence of a Weyl node allows the existence of massless, quasiparticles known as Weyl fermions, named for Hermann Weyl who first theorized their existence in 1929 [3, 4].

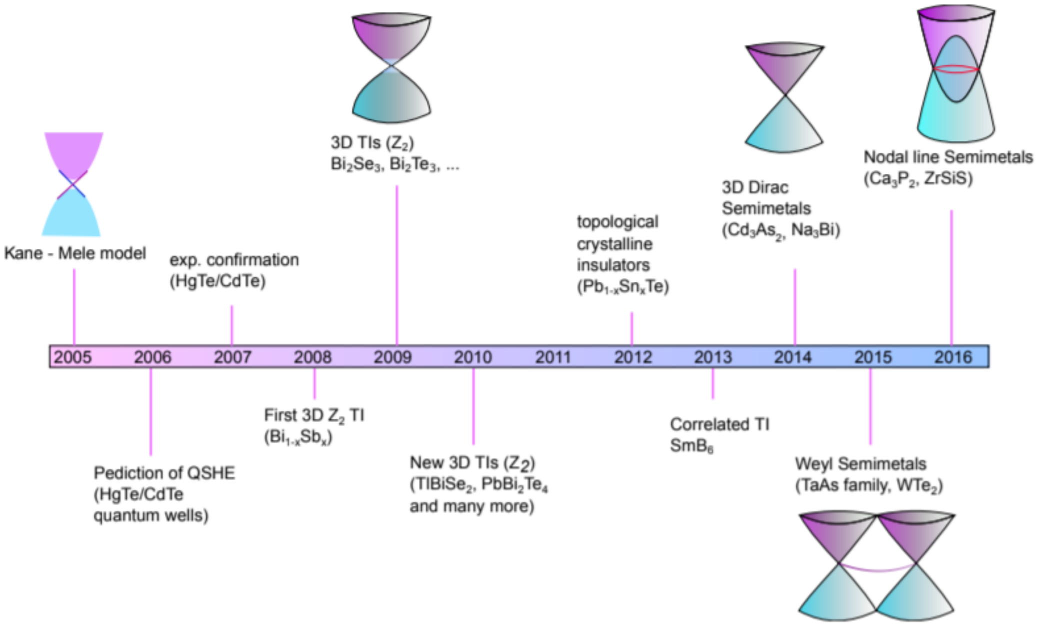

Figure 1.1. Historical timeline of the field of topological insulators and semimetals [5].

Weyl fermions, however, can only exist in materials which have overlapping band gaps, and which lack either inversion or time reversal symmetry [6-8]. Figure 1.2 graphically represents bands of several types of topological materials, including Weyl semimetals. Put respectively, inversion symmetry means the crystal has a geometric inversion center, and time reversal symmetry means the material shows no phase transition. Due to mathematical consequences of the quantum mechanical Pauli matrices, Weyl nodes are stable in three dimensions and allow electrons to travel topologically in paths known as Fermi arcs—in other words, Weyl nodes allow the materials to conduct electricity, but only along their surfaces, dramatically reducing resistance and waste heat [9].

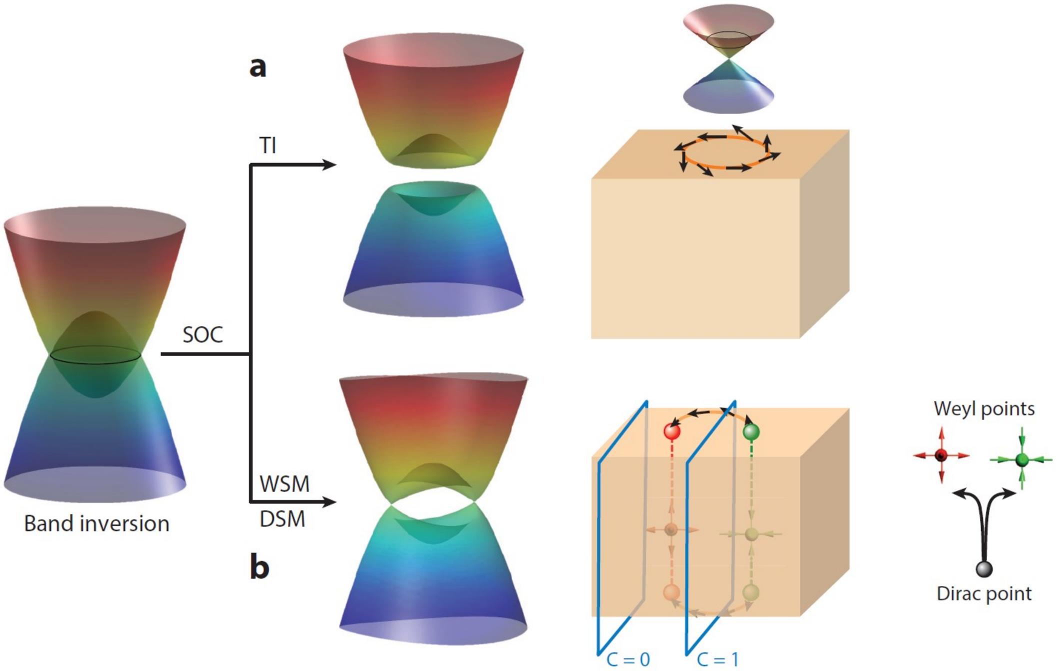

Figure 1.2 Variations on spin orbit coupling and band gaps for (a) topological insulators, and (b) Weyl or Dirac semimetal [10].

Band theory suggests that materials can be classified in several broad groups based on the behavior of their so-called, “band gaps”. The groups include insulators, conductors, metals, semimetals, and semiconductors. In an insulator, a larger amount of energy is needed to have electrons bridge the band gap between the conduction and valence bands. Aside from the general groups discussed above, certain subtypes can be determined based on certain types of band interactions. Some insulators with specific band gap formations (see Figure 1.2a) can create a topological insulator. Others, which are of more direct interest to this research, can form a Weyl semimetal (see Figure 1.2b). The conical stalactite-stalagmite type of formation occurring band gaps shown in Figure 1.2 is known more commonly as a “Dirac cone”. For the material to be a Weyl semimetal, the two Dirac cones must approach each other at two points, but not overlap. Then, electricity can travel topologically across the material [11].

The desirable aspects of topological conduction, notably including the reduction of waste heat, have led to much research in the past decade in an attempt to discover topological materials which can be used in practical, electronic applications. Such applications include immediate use in microelectronics or computers where waste heat is of great importance. Yet, topological semimetals could also be used in more exotic locations, such as electronics that need to operate at very low temperatures or, if perfected, topological materials could be used to coat normally non-conductive materials, thereby turning them into conductors without the need for the entire bulk of the material to be conductive. Finally, many topological semimetals show high carrier mobility and significant linear magnetoresistance; fine-tuning such material properties may help develop new “spintronic”-type devices which also demonstrate a lower-than-normal rate of power consumption [12].

Recent research has demonstrated that bismuth can form topologically insulative, binary materials when prepared with a flux growth method [13]. Bismuth is also readily available, nontoxic, and can react in a variety of charge balances. For all the above reasons and others, bismuth was used as a flux material for the first set of flux growth reactions in this project as well as in many later reactions. In flux growth, reactants are mixed together, usually in powdered forms, with a much higher concentration of another element, the flux, and then cooked in a furnace while the reactants and flux are contained within an evacuated atmosphere—usually down to 3-5 milliTorr [13-14].

When selecting elements to be combined, conductive/magnetic metals (e.g. iron or cobalt) were chosen and also selected ingredients that could combine in a charge-balanced manner. Topological semimetals are charge-balanced compounds, unlike topological insulators. In the most recent, apparently successful growths, stochiometric ratios were used, similar to those used elsewhere [15-16]. In these targeted reactions, of which there are roughly 30, we had success in growing Sm_3HfBi_5, a material which at the time of the synthesis was undiscovered. Since then, however, it has been reported on [15]. Several, focused, yet still-exploratory reactions were used, before narrowing down attempts at growth to Sm_3HfBi_5, which will be characterized below. To date, there is no in-depth characterization of Sm_3HfBi_5. Thereby, this thesis advances the field of topological materials research by characterizing a new material.

METHODS

Flux Growth:

Before discussing the specific sets of reactions performed for this research, it would first be worthwhile to discuss the flux crystal growth method in detail. The first step of crystal formation is known as “nucleation”. Nucleation can occur either within the bulk of a material or at the interface between two materials such as the boundary between a liquid and its container, the bulk and the air, or around an impurity in the bulk material. Josiah Willard Gibbs was the first to develop a formula describing the path of small structures coined, “nuclei”, that grow into macroscopic crystals [17]. A special case of the Gibbs-Thomson equation assuming there is constant pressure during the nucleation process is:

$$k_B T \ln\left(\frac{C}{C^*}\right) = \frac{2\sigma V}{r}$$

Equation (2.1) Constant Pressure Gibbs-Thomson equation

where C is the actual concentration, C^* is the concentration of the solution with a crystal of infinite radius r, k_B is the Boltzmann constant, σ is the surface energy per unit area, V is the volume of the growth units, and T is the temperature of the crystal. Figure 2.1 provides an intuitive demonstration of crystal growth. It illustrates three zones. The lowest zone on the figure is the stable zone where crystallization is not thermodynamically feasible. The middle zone is the metastable zone where spontaneous crystallization is improbable. Finally, the third zone is the unstable zone where spontaneous crystallization is possible or even probable, but not guaranteed.

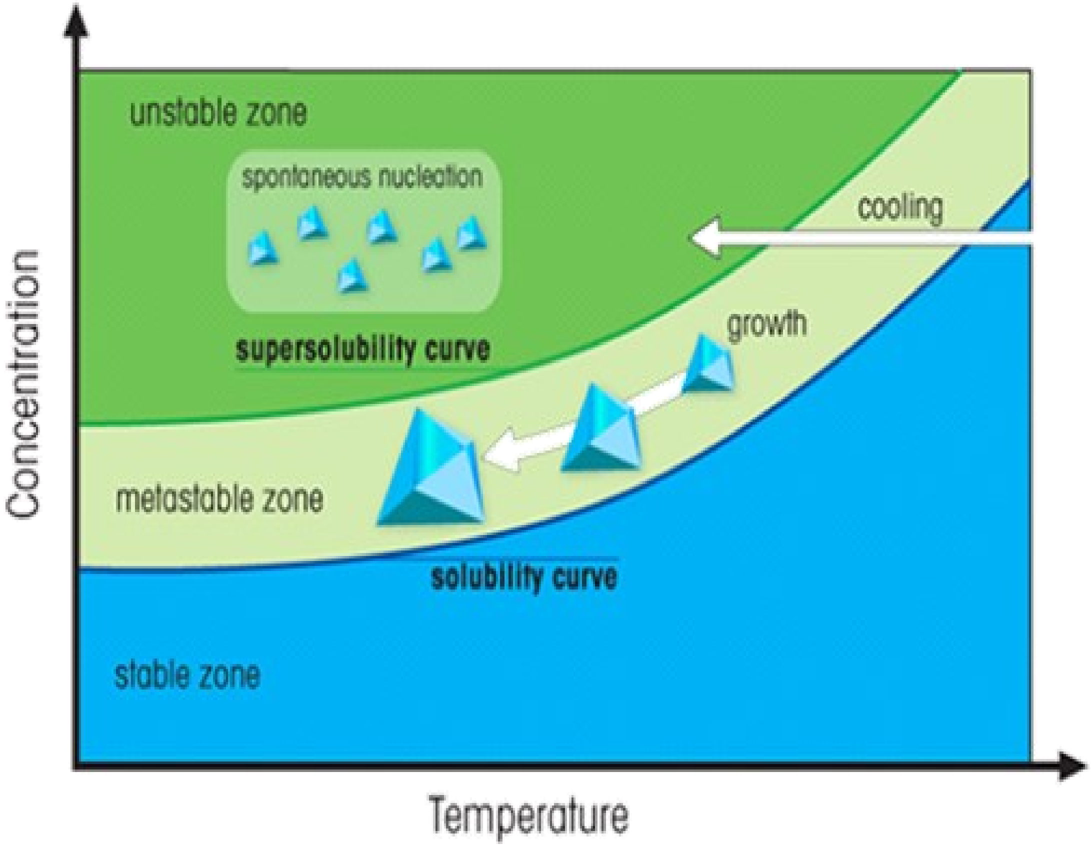

Figure 2.1 Thermodynamics of crystal growth [18].

Theoretically, crystallization can begin when the concentration of a compound in a solvent just surpasses the solubility limit of that solid in that solvent. Beyond theory, the crystallization process is impeded kinetically, and therefore crystals usually grow only from supersaturated solutions. Slowly cooling the supersaturated solution can aid in the crystallization process as temperature of solvent decreases, so does its solubility limit and more material can precipitate out into or onto a crystal. When cooled too rapidly, widespread nucleation results in the growth of too many, too small crystal nuclei—when in flux growth usually crystals of a larger size are desired. Cooling slowly limits the number of crystal nucleation sites.

There are several types of possible growth techniques. To illustrate the sheer variety of techniques available, there is a helpful diagram in Figure 2.2 [19].

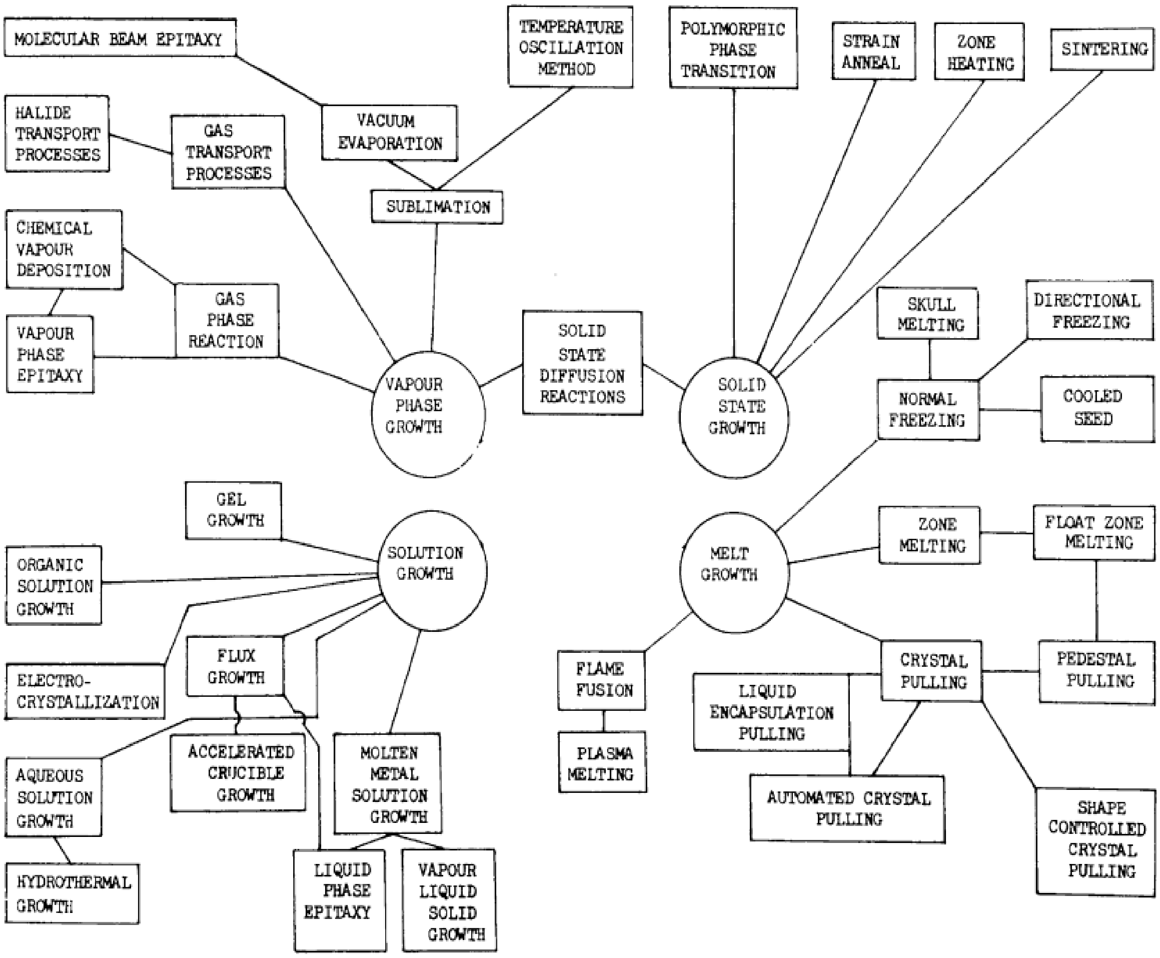

Figure 2.2. Crystal growth techniques [19].

The method most relevant to, and used in, this research is known as flux crystal growth. Pamplin describes it as a subset of solution growth which is itself a subset of melt growth. According to Pamplin, the main differences between melt and solution growth are that in melt growth, the solvent freezes well below its melting point. While, in solution growth, the solute crystallizes well below its melting point [19]. Both melt and solution growth can be useful when trying to crystallize substances that melt at different temperatures—while using relatively simple equipment such as a furnace and crucible.

In flux crystal growth many elements are combined in a container, often referred to as a crucible. One of the materials is present in a much larger proportion than the other. It is this material, present in a greater amount, that is called the “flux”. The flux should melt and form a bulk material in which the flux and other materials may nucleate and then grow into other crystals. In the reactions pertaining to this research only pure elements were mixed within the crucibles. There were several iterations of reactions which are discussed in greater detail below. In general, however, the elements were weighed out on a balance scale and then loaded into the crucibles. Two identical cylindrical, alumina crucibles were used for each growth (see Figure 2.3). The bottom crucible held the chemicals and the top crucible held quartz wool.

Figure 2.3 A set of alumina crucibles used for reactions.

The reactants with the lowest atomic weight were measured and put into the crucibles first. Those reactants with the second-lowest atomic weight were put into the crucible next, and so on. If a reaction contains air-sensitive, rare-earth elements these were loaded into the crucibles inside an inert, argon-atmosphere glovebox. After all the reactants have been loaded into the crucibles, the flux is added to cover the other reactants.

Quartz wool was loaded into the top crucible inside the glovebox to minimize the amount of trapped air. The wool acts as a filter letting through molten flux, “catching” crystals during centrifuging (see below). The top crucible rested upside-down on the chemical-containing crucible as a cap. The crucible ensemble was inserted into quartz ampoules and connected to a Schlenk line in connection with a turbo pump (see Figure 2.4).

Figure 2.4. The glovebox (left) and Schlenk line setup (right).

After pumping the air down to below 5 milliTorr, a hydrogen-oxygen torch was used at the Schlenk line to seal off the crucible ensemble by melting the quartz ampoule above the ensemble. Figure 2.5 shows a reaction ready for the furnace. In many reactions, the vacuum pump is left on while sealing to keep the tube as evacuated as possible during the sealing process. In some later reactions, notably 107 and 108, we use an additional attachment to the Schlenk line to sustain a method known as “argon backfill”. Put simply, instead of sealing the crucibles with a vacuum on the inside, pure argon is allowed to flow into the ampoule while sealing.

One must be careful to balance correctly the argon back pressure inside the ampoule. Too much, and the heated argon gas can cause the ampoule to explode while being heated and sealed with the torch. Too little, and the ampoule seals as if under vacuum. The switch to argon backfill can be explained for two main reasons. The first is that sealing under vacuum is an incredibly difficult process causing ampoules to break about as often as it succeeds in sealing them. Argon backfill allows for greater chance of error as the glass of the ampoule is much less likely to bubble inwards and then suddenly pop—if there is argon gas inside the ampoule providing back-pressure.

The second main reason for switching to argon backfill is a puzzling difficulty in growing Sm_3ZrBi_5, one of the compounds replicated easily elsewhere [2]. The only apparent difference in our growth method was we were not equipped with an argon backfill system during the exploratory growth portion of the project. After adding the argon backfill system, numerous reactions were still unable to grow Sm_3ZrBi_5. The argon backfill also seemed to cause an increase in the number of reactions which oxidize—a failure of the crystallization process where oxygen gets into the ampoule and causes common oxide-compounds to form in lieu of the more rare, more sought-after ternary intermetallics. Many attempts were made to improve seals along the argon backfill system as well as imposing a water-filter, more commonly known as a "bubbler" at the end of the argon line. In the end, however, no instances of Sm_3ZrBi_5 were grown while attempting the argon backfill system. Nor were any crystals of the titular compound, Sm_3HfBi_5. Most likely, the difficulty with argon-backfill results from an equipment issue. There must be a leak either during the sealing process under argon back-pressure, or in the line/joints connecting the argon canister to the ampoule. Additionally, our monitoring equipment can measure a flow-rate, but not provide an exact pressure in the ampoule.

Figure 2.5 A fully sealed reaction ready for the furnace. The bottom alumina crucible contains the chemicals and the top crucible contains quartz wool that will act as a filter.

Returning to the general method used in flux crystal growth, after sealing the ampoule each set of reactions is placed into a programmable furnace. Although some variation can be used in what temperature profile runs, e.g. if one is trying to grow a specific material, in cases where growths are considered “exploratory”, a standard program is used. Over the course of about 10 hours, the furnace heats up to 1,000°C. The program keeps the furnace at that temperature for roughly 10-20 hours allowing for the reactants to soak in the melted flux. The furnace is then slow-cooled at a rate between one and five degrees per hour, until about 50-100°C above the flux melting/solidification point ensuring the flux will remain liquid during extraction and centrifuging.

In our more focused sets of growths where the growths targeted specifically Sm_3HfBi_5 and Sm_3ZrBi_5 a slightly different program was used. Most often the tubes were placed in box furnaces, heated to 1000°C over the course of 10 hours, held there for roughly 10 hours, and cooled over the course of 72 hours to 700 °C. At 700 °C, the ampoules were taken out of the furnace and centrifuged. Owing to the great difficulty in growing Sm_3HfBi_5, some variation was used while attempting the growth in order to see if growing parameters might be optimized. In one growth, the crystals were left to cool slowly down from 1000 °C to 700 °C over the course of two weeks. In another, the crucible caps were removed. In another, the caps were left on. In some, the ternary reaction was grown in vacuum down to 0.3 milliTorr. While in yet others, argon backfill was attempted.

In either case, the reactions are set to rest at a certain temperature for several days. The final resting temperature, however, changes with each set of reactions, and can only be determined after consulting the phase diagrams of several known binaries between the reactants and flux. The goal is to keep the final resting temperature high enough that the flux material stays liquid when centrifuged. When the furnace settles on a final resting temperature, the reactions are quickly removed from the furnace, flipped upside down with tongs, and immediately centrifuged. The centrifugal force pulls the liquid through the quartz wool while the wool catches most crystals produced in the process, which is designed to ensure separation between the soon-to-be solid flux and the crystals.

After allowing the ampoules to cool down to room temperature—so they are safe to handle—the ampoules are then broken open and the crystals inside are harvested. Crystals are most readily identified under the microscope by their regular geometry, and often by being reflective. Any promising candidates are then put onto copper tape and examined in a scanning electron microscope equipped with energy dispersion spectroscopy (EDS) for elemental identification and composition.

If EDS suggests the crystals may be novel materials, both powder and single crystal x-ray diffraction are utilized to determine the final structure. These analytical methods are more fully discussed later in the results section of this paper.

Reactions:

In total, 52 reactions were performed as part of this research. In the exploratory phase of research, five sets of reactions were completed. It total, there are 25 reactions represented in the exploratory phase. The second phase of research can better be described as reactions focused on the growth of bismuth-based crystals of the rough form Ln_3MBi_5; where Ln refers to a lanthanide, M refers to a metal and Bi, of course, refers to bismuth. There have been 27 reactions performed in this focused set. Each phase of the research reactions is detailed below, as well as provide context for why each set was chosen.

Experimental Reaction Phase:

Three sets of the experimental reactions used bismuth as a flux with transition metals and rare earths as the other starting materials. One set of reactions used tellurium as a flux along with nickel and rare earths. The final set used indium as a flux with phosphorous, manganese, and rare earths as starting materials. Every set of these exploratory reactions created crystals, many of those crystals, however, were known binaries. In some cases, the reactions created unwanted, oxidized crystals or samples. None of these binaries or oxidized materials were, in point of fact, novel materials.

The first step in any reaction is to decide what materials will be used and in what ratio. With few exceptions, one millimole of each reactant and ten millimoles of each flux were used in the first phase of exploratory reactions. The only exceptions to this standard mix are: using ten millimoles of boron due to its extremely low atomic weight, and, using 20 millimoles of indium, rather than ten, when using indium as a flux. For greater clarity, see Tables 2.1, 2.2 and 2.3, below.

Table 2.1: First sets of exploratory reactions in this study.

Set 1 Reaction “61”, 1-4	10 mmol (flux)	1mmol		1mmol
	Bi	Fe		Nd
				Eu
				Ho
				Yb
Set 2 Reaction “61”, 5-9	10 mmol (flux)	1mmol		1mmol
	Bi	Co		Nd
				Eu
				Ho
				Yb
Set 3 Reaction “69”, 1-5	10 mmol (flux)	1mmol		1mmol
	Bi	Mn		Ce
				Nd
				Gd
				Ho
				Tm
Set 4 Reaction “72”, 1-5	10 mmol (flux)	1mmol	1mmol	10mmol
	Te	Ni	Ta	B
			Hf	B
			Ta	
			Hf	
			Fe	Sn (1mmol only)
Set 5 Reaction “77”, 1-6	20 mmol (flux)	1mmol	1mmol	1mmol
	In	P	Mn	Fe
				Ru
				Os
				Re
				Pd
				Au

Table 2.2: Second sets of focused reactions.

	20 mmol (flux)	3 mmol	1 mmol
Set 1 Reaction “89” (1-6)	Bi	Sm	Zr
			Hf
			Ti
		Eu	Zr
			Hf
			Ti
Set 2 Reaction “91” (1-5)	Bi	Sm	Zr
			Hf
			Mn
			Nb
			Mg
Set 3 Reaction “107” (1-4)	Bi	Sm	Hf
			Hf
			Zr
			Zr
Set 4 Reaction “108” (1-4)	10mmol	1.5 mmol	0.5 mmol
	Bi	Sm	Hf

Focused Reaction Sets:

The second main type of reactions in this study have been reactions focused on growing the Ln_3MBi_5 type of crystals as described in Ref [2]. This class of materials is extremely air-sensistive and testing almost always destroys the crystal being examined—more on air sensitivity, below. Such a fragile crystal requires many attempts at growth not only to optimize the routine for a successful growth, but also to replace crystals lost during the characterization process.

The flux growth method is still used, as described above. Some variations in the technique described above include different furnace heating routines and attempts at growing under argon backfill. Two main types of crystal, Sm_3ZrBi_5 and Sm_3HfBi_5, were attempted to be grown as shown in Table 2.3, below.

Sets 1, 2, and 3 were sealed under vacuum only, heated to 1,000°C over 20 hours, left at 1,000°C for 24 hours, and then cooled to 700 °C over 100 hours, then centrifuged. Set 3 was sealed under Argon backfill, heated to 1,000°C over 20 hours, left at 1,000°C for 24 hours, and then cooled to 700 °C over 100 hours, then centrifuged. Set 4 was sealed under argon backfill, heated to 1,000°C over 20 hours, left at 1,000°C for 24 hours, and then cooled to 700 °C over 300 hours, then centrifuged. For set 6 and 7, the crystals were sealed under vacuum only, heated to 1,000°C over 20 hours, left at 1,000°C for 24 hours, and then cooled to 700 °C over 100 hours, then centrifuged.

Table 2.3: Focused reactions.

Set 1 Reaction “89”, 1-6	20 mmol (flux)	3 mmol	1 mmol
	Bi	Sm	Zr
			Hf
			Ti
		Eu	Zr
			Hf
			Ti
Set 2 Reaction “92”, 1-5	20 mmol (flux)	3 mmol	1 mmol
	Bi	Sm	Zr
			Hf
			Mn
			Nb
			Mg
Set 3 Reaction “107”, 1-4	20 mmol (flux)	3 mmol	1 mmol
	Bi	Sm	Hf
			Zr
Set 4 Reaction “108”, 1-4	20 mmol (flux)	3 mmol	1 mmol
	Bi	Sm	Hf
Set 5 Reaction “114”, 1-4	20 mmol (flux)	3 mmol	1 mmol
	Bi	Sm	Hf
Set 6 Reaction “115”, 1-2	20 mmol (flux)	3 mmol	1 mmol
	Bi	Sm	Hf
Set 7 Reaction “117”, 1-2	20 mmol (flux)	3 mmol	1 mmol
	Bi	Sm	Hf

RESULTS

As stated above, the project has grown crystals on every set of reactions. The majority of the crystals, unsurprisingly for exploratory research, have largely not been novel materials. The section below summarizes the results from the earliest reactions onward and characterizes, to what extent has been possible, the titular compound of this paper, Sm_3HfBi_5, a new, seemingly topological material. Initial magnetization and crystal structure data results have been collected,

It is worth noting at the beginning of this section that, often, reactions have oxidized in the furnace. Many attempts and alterations have been made to the Schlenk line to prevent oxidation including a complete rebuild swapping out glass for a custom stainless-steel line and the addition of the argon backfill method, described in more detail above. The question "where is the oxygen coming from?" is one that the research team is constantly fighting as the reactions are sealed under vacuum and primarily use materials that have been left in an argon atmosphere for days or weeks before sealing. They are always sealed either in tubes that have been left evacuated for several minutes or filled with argon for a similar duration of time.

Exploratory Reaction Results:

The first, exploratory reactions did not produce novel materials. Figure 3.1 showcases several crystals grown during the early stages of the research project. There are pictures of a pure cobalt crystal that grew into a pyramid structure. Also included are two images of indium oxide. These images demonstrate many of the characteristics one looks for when trying to find crystals in the flux material after a reaction. They are faceted, reflective, and geometrically regular. The two indium oxide samples also illustrate that the same material can take different shapes or colors.

Finally, one of the sets of indium oxide crystals shows a common characteristic of oxidized crystals. Namely, that they are often transparent and brightly colored—though as the rectangular indium oxide crystals show, this is not always the case.

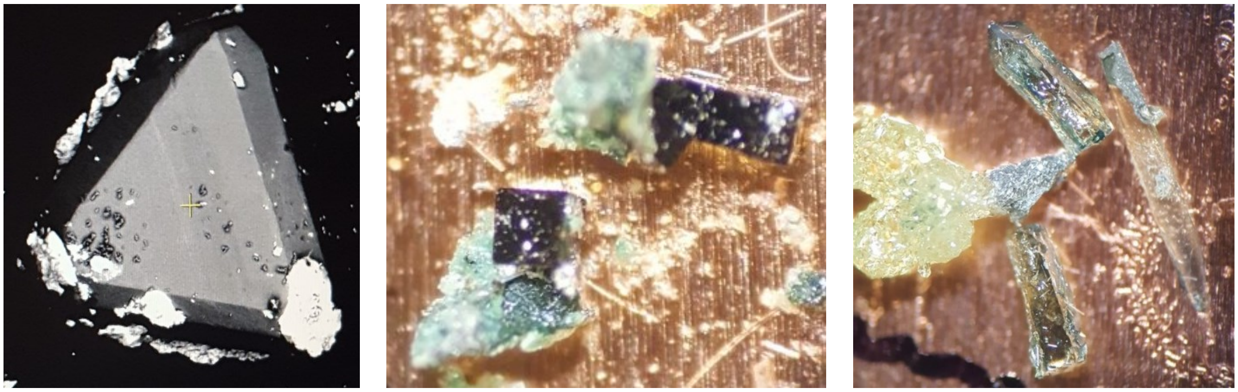

Figure 3.1. (left) SEM images of a pure cobalt crystal; (center and right) optical microscope images of several indium oxide pictures.

Focused Reaction Results:

The second set of reactions produced several oxidized reactions, but these sets of reactions also produced two successful growths of Sm_3HfBi_5. It is a rod-like, hexagonal crystal which often grows to be several millimeters long. Figure 3.2 shows the crystals immediately after they have been removed from the sealed ampoule. At first, Sm_3HfBi_5 crystals seem quite rigid—they will not break even when squeezed with steel tweezer. The compound, however, is quite air sensitive and begins to degrade after only a few hours in regular atmosphere. See Figure 3.3 for the images of the material breaking down. Samples were kept stable as rods inside and argon-atmosphere glovebox for several months. Many of these characteristics are verified elsewhere. [2, 5, 16] The air-sensitive nature of Sm_3HfBi_5 made taking several, typical characterization measurements on the crystals difficult. Nevertheless, we were able to perform single crystal x-ray diffraction on the crystals to help determine the structure of Sm_3HfBi_5 and were able to have another lab perform magnetic analysis on the crystals.

Figure 3.2. Sm_3HfBi_5 crystals immediately after breaking open a reaction.

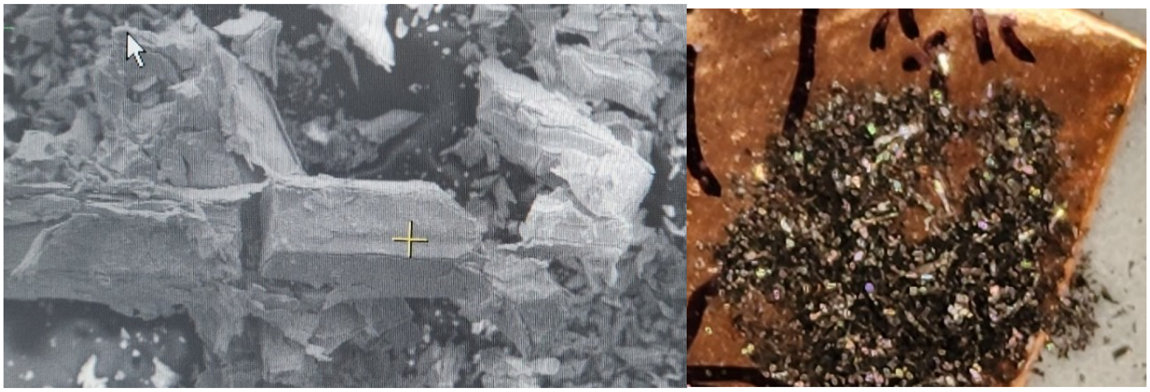

Figure 3.3. Sm_3HfBi_5 after only a few hours exposure (left) during SEM measurements, and the same rod, reduced to dust overnight (right).

Single Crystal X-ray Diffraction:

Analysis using X-ray diffraction relies on the constructive interference of monochromatic x-rays and the atomic lattice of a sample crystal. When conditions satisfy Bragg's law

($n\lambda=2d\sin\theta$), the intensity of measured x-rays spikes. A graph of intensity on the y-axis and a value of 2θ on the x-axis is typical for a powder x-ray diffraction. Figure 3.4 shows a typical graph from a power x-ray diffraction. The information in the figure is artificial, however, as it is generated by the software VESTA from single-crystal x-ray diffraction data. No successful powder x-ray diffraction data was collected for Sm_3HfBi_5. The material rapidly degrades in air when whole. Grinding it up into a powder accelerated the process to such a degree that the time required for powder x-ray diffraction, yielded no meaningful data. The crystal lattice had been destroyed before a full sweep of 2θ values could be completed. Because the constructive interference depends on the geometry of the crystal, information about the structure of a crystal can be determined by processing at which points the "spikes" of intensity occur.

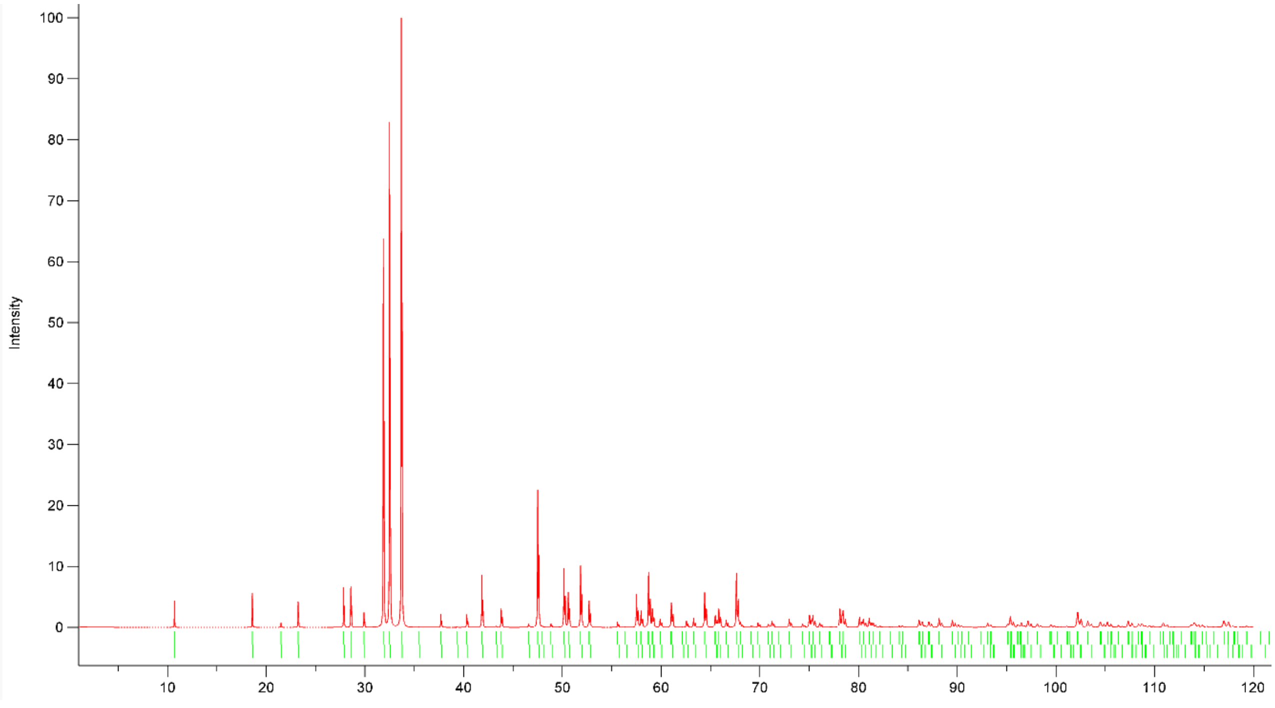

Figure 3.4 "Powder" x-ray diffraction pattern generated from single crystal x-ray diffraction data.

In single-crystal x-ray diffraction, the same idea of constructive interference between incident x-rays and the sample's crystal lattice applies, the difference being that single-crystal x-rays often collect data from a three-dimensional field. The resulting data looks less like "spikes" in intensity on a two-dimensional graph, and more like bright spots of intensity on a 3D dimensional projection—a fitting analogue is stars mapped onto the inside of a sphere. This diffraction pattern can be fed through software and used to calculate structure as well. The structural parameters obtained from single crystal x-ray analysis of Sm_3HfBi_5 are shown in Table 3.1. The data was collected at room temperature. Table 3.2 shows the expected atomic coordinates of Sm_3HfBi_5.

Information from the single-crystal x-ray diffraction can be collected into an electronic filed known as a .cif file—short for crystallographic information file. The .cif file contains all the structural information of a particular crystal. Several software packages exist that can generate images from a .cif file. For the images below, the free software known as VESTA was used. Figures 3.5 and 3.6 show the crystallographic structure of Sm_3HfBi_5 as based on single crystal x-ray diffraction. In all cases bismuth is colored light blue, samarium is pink, and hafnium is yellow.

Table 3.1: Single crystal X-ray diffraction data and parameters for Sm_3HfBi_5, collected at room temperature.

Parameters	**Sm_3HfBi_5**
Molecular weight (g/mol)	1674.59
Space group	$P6_3/mcm$ (#193)
a (Å)	9.5386(2)
c (Å)	6.4049(3)
V (Å^3)	504.68(2)
Z	2
ρ_{calc} (g/cm^3)	11.019
Absorption coefficient μ (mm^{-1})	114.132
Crystal size (mm^3)	0.091 x 0.102 x 0.114
Data collection range (°)	$2.466 < \theta < 44.798$
h range	$-18 \leq h \leq 18$
k range	$-18 \leq k \leq 18$
l range	$-12 \leq l \leq 12$
Reflections collected	77227
Independent reflections	784
Parameters refined	14
R_{int}	0.024
$R_1(F)$ for all data[a]	0.0503
$wR_2(F_O^2)$[b]	0.1341
Goodness-of-fit on F^2	1.0000

[a] $R_1 = \Sigma \| F_O | - | F_C \| / \Sigma | F_O \|$.

[b] $wR_2 = [\Sigma w(F_O^2 - F_C^2)^2 / \Sigma w(F_O^2)^2]^{1/2}$, $w = 1/[\sigma^2(F_O^2) + (A \cdot P)^2 + B \cdot P]$, $P = [2F_C^2 + \mathrm{Max}(F_O^2,0)]/3$ where $A = 0.08$ and $B = 38.24$.

Table 3.2. Atomic coordinates, and equivalent displacement parameters of Sm_3HfBi_5.

Atom	SOF	Site	x	y	z	U_{eq} (Å^2)
Bi1	1	6g	0.26614(6)	0	1/4	0.0097(20)
Bi2	1	4d	1/3	2/3	0	0.0102(20)
Sm	1	6g	0.61821(9)	0	1/4	0.0114(3)
Hf	1	2b	0	0	0	0.0116(4)

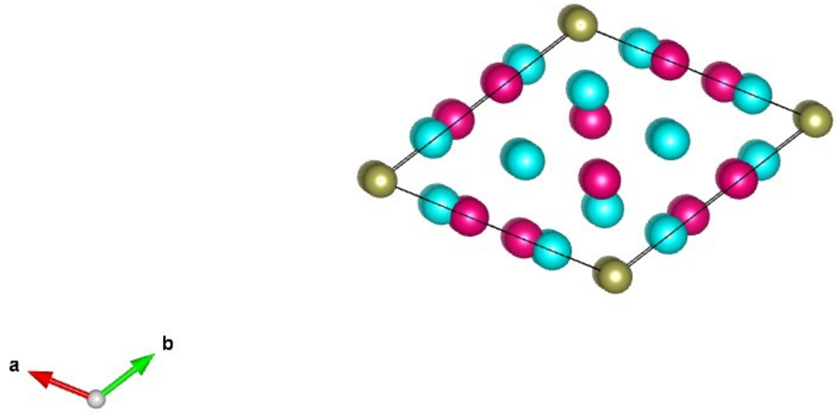

Figure 3.5. Looking down the length of the c-axis, or down the length of the rod.

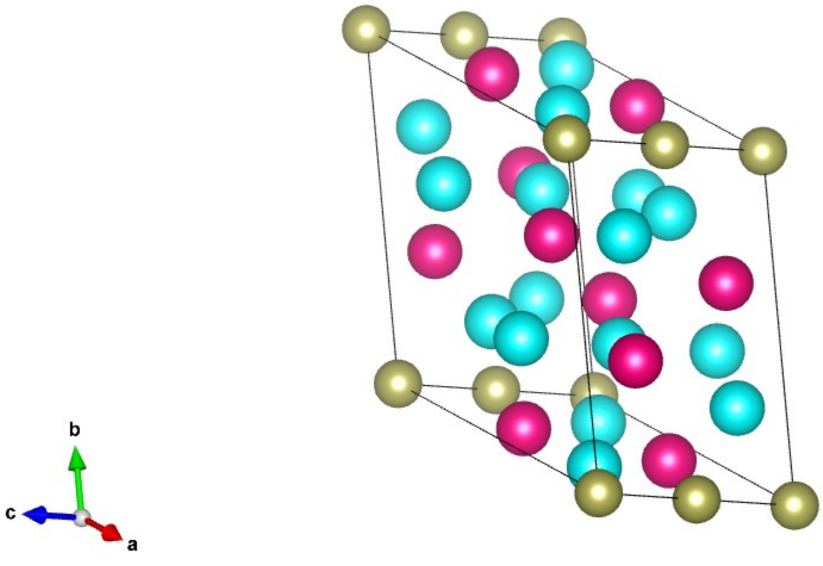

Figure 3.6. The unit cell of Sm_3HfBi_5.

Magnetic Characteristics:

Magnetism is one of the most important qualities to be measured in novel materials. The literature, however, is far from uniform in its choice of units, variables, or its approach to magnetism. This paper uses as a basis the illuminative work of Mugiraneza and Hallas [20]. A measurement of prime importance is the equation relating a material's magnetization to its magnetic susceptibility.

$$M = \chi H$$

Equation (3.1) Magnetization and magnetic susceptibility

Where, in Equation 3.1, M is equal to the magnetization, χ is equal to the magnetic susceptibility and H is equal to the applied, external magnetic field. Magnetic susceptibility measurements can provide information on how a material responds to an applied magnetic field, which can be used to develop a magnetic characterization of a material. [20] Figure 3.7 shows the measured magnetic susceptibility of Sm_3HfBi_5. The susceptibility is measured at a variety of changing temperatures which form the x-axis of Figure 3.7.

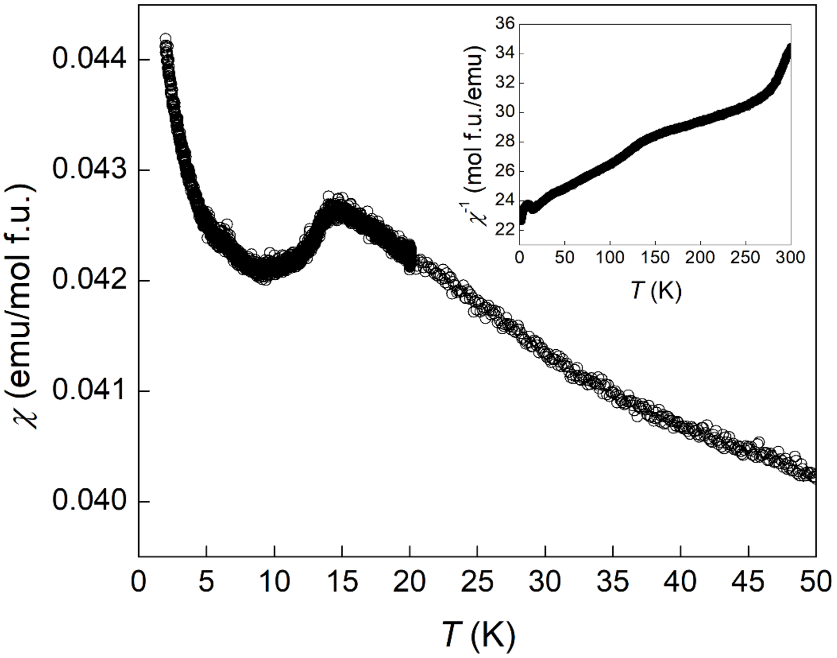

Figure 3.7. Magnetic susceptibility of Sm_3HfBi_5 and inverse susceptibility (upper right).

Though in common parlance materials are often referred to as “magnetic” or “nonmagnetic”, in materials characterization there are several subtypes of magnetism which need here require further elucidation. Fundamentally, magnetism depends on a property of matter called “spin”. Spins of different particles or groups of particles can align, creating an area of uniform magnetism called a “domain”. Domains express a magnetic potential in a certain direction. Many materials have magnetic domains pointed in a variety of directions, and the sum magnetization of a material depends in part on the susceptibility of the material but also on the orientation of these magnetic domains. Some arrangements of magnetic domains have earned their own names. Most familiar are perhaps ferromagnets, which, at certain temperatures, exhibit uniform alignment in a magnetic field—and often retain this alignment for some time after the magnetic field is removed. Such is the common bar magnet. Ferromagnetism—in fact all magnetism—however is also partly dependent on temperature. Ferromagnets lose their “permanent” magnetic properties above a temperature known as the Curie temperature (T_C). The energy of heating will overcome the magnetic force aligning all the individual domains of a ferromagnet and the domains will point in a random distribution of directions. Ferromagnetic materials generally recover the uniform domain if cooled below the Curie temperature and are again exposed to a strong enough external magnetic field. A material in which thermal motion has randomly oriented the magnetic domains is called “paramagnetic”. Paramagnets showcase a slight magnetization within an external magnetic field, but do not retain this magnetism when the field is removed. A special case of spin alignments, where alternating layers of a material have directly opposing spins is called “antiferromagnetic”. In the simplest case of an antiferromagnetic material, one layer of a crystal lattice would have spins pointing “straight up” and in the next layer the pins would be pointing “straight down”, and so on. In reality, antiferromagnetism can be observed in more complex orientations. In the final case to be discussed here there is also a state in between ferromagnetism and antiferromagnetism called “ferrimagnetism”. In a ferrimagnet, some of the magnetic moments are aligned in one direction, while others are aligned in the opposite direction, but there is an overall imbalance that results in a net magnetization.

Returning to Figure 3.7, we are now better equipped to interpret its results. At roughly 15K there is a spike in the susceptibility data which indicates an antiferromagnetic transition. Antiferromagnetic transitions occur at a critical temperature, known as the Neel temperature (T_N), which is specific to each antiferromagnetic material. Below the Neel temperature, the material exhibits antiferromagnetic order, where adjacent magnetic moments are aligned in opposite directions, canceling each other out. This leads to a lack of macroscopic magnetization in the material—and the subsequent dip in magnetic susceptibility observed below 15K. The magnitude of the change in magnetic susceptibility at this transition is small. In Sm_3HfBi_5 only Samarium can introduce this kind of antiferromagnetic transition. It is possible that the material may be ferrimagnetic, but the data is inconclusive. Looking at the smaller graph in Figure 3.7, we see the inverse susceptibility plotted against the temperature at which measurements were taken. A straight line on such an inverse susceptibility graph would show evidence of Curie-Weiss behavior, common in paramagnetic materials. Sm_3HfBi_5 shows no evidence of Curie-Weiss behavior. It is likely that the bulk of our sample was degraded by the time these magnetic measurements were taken. The small antiferromagnetic transition observed at roughly 15 K was likely due to a small amount of sample still intact.

Comparing Sm_3HfBi_5 to other similar materials in extant literature, we find dissimilar observations for susceptibility made of La_3HfBi_5—which behaves like a Pauli paramagnetic material with all-positive susceptibility values that are temperature-independent down to 1.85K [21]. As shown below in Figure 3.8.

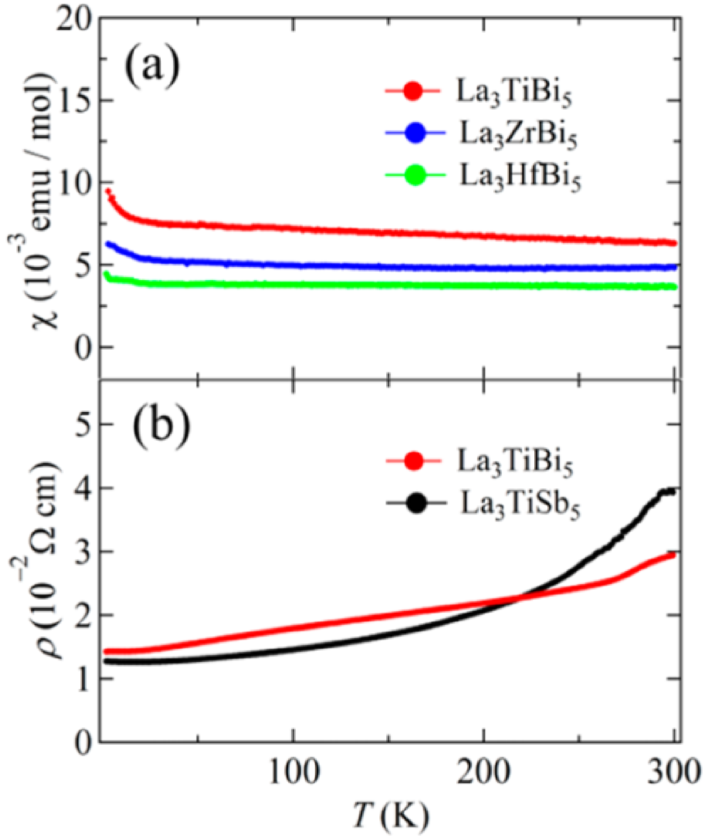

Figure 3.8. Magnetic susceptibility and resistivity values of La_3HfBi_5 [21].

A similar antiferromagnetic transition to that observed in Sm_3HfBi_5 occurs at roughly 16K in Sm_3TiSb_5—see Figure 3.9 [22]. The researchers in this study note that Sm_3TiSb_5, like Sm_3HfBi_5, also does not show Curie-Weiss behavior. Moore, et al. suggest the behavior may be explained by "the samarium 4f electrons interacting with the conduction electrons to form a magnetic ground state that is favored over a superconducting phase" but suggest the "loss of spin-disorder scattering accounts for the abrupt decrease in resistivity below 16 K." [22].

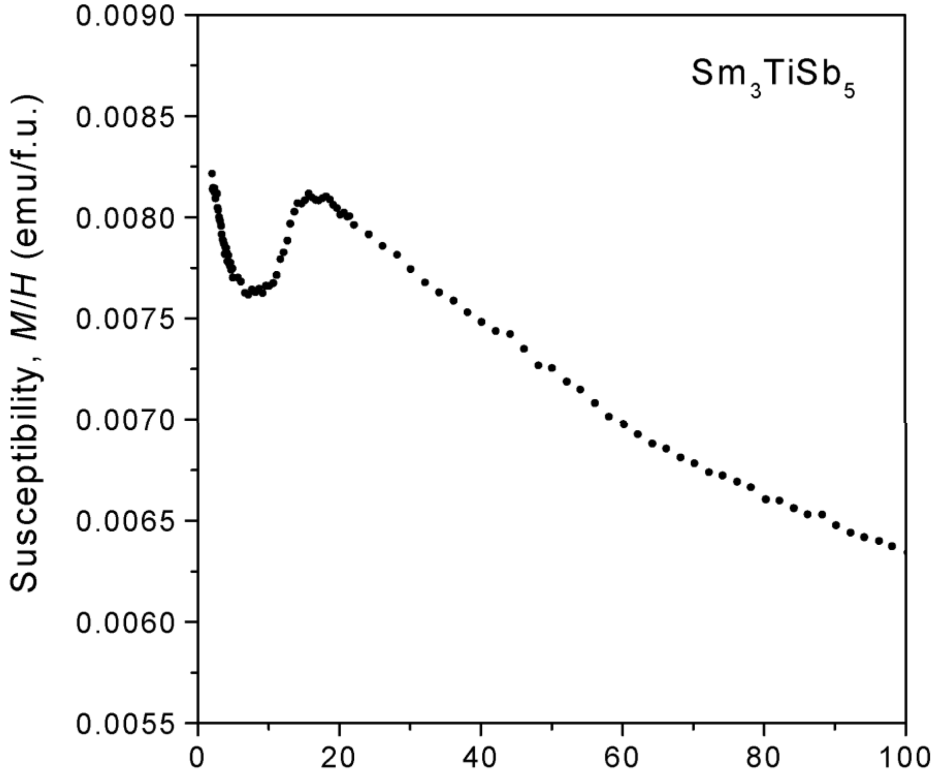

Figure 3.9. Magnetic susceptibility of Sm_3TiSb_5 [22].

When comparing Sm_3HfBi_5 to Sm_3ZrBi_5 there are antiferromagnetic transitions occur in roughly the same temperature range, but the change of magnetic susceptibility in Sm_3ZrBi_5 has a greater magnitude. In Figure 3.10 the blue line with the larger antiferromagnetic transition shows the magnetic susceptibility as measured along the length of the rod. The orange line with the much smaller antiferromagnetic transition shows the magnetic susceptibility as measured perpendicular to the rod. In all other figures showing magnetic susceptibility, the susceptibility has been measured along the length of the rod. Khoury et al. suggest their sample's magnetism is largely the result of Sm^{3+} cations interacting with each other to generate paramagnetic behavior in the first excited state [15]. To quote, "The fitted magnetic moments (μ_{eff}) are 1.18 and 1.34 μ_B/mol Sm when the field is applied parallel and perpendicular to the c axis, respectively. These moments are higher than the predicted free-ion value of 0.85 μ_B for a Sm^{3+} cation or those observed in some Sm compounds, such as Sm-pyrochlores." [15]. When measuring Sm_3HfBi_5, we found roughly ~0.03 μ_B /mol Sm. The significant difference in observed values between Sm_3HfBi_5 and Sm_3ZrBi_5 could be due to sample degradation. Such a difference could also be due to Sm_3HfBi_5 being formed with the Sm^{2+} cation which is non-magnetic with a free-ion value of 0 μ_B rather than the magnetic Sm^{3+} cation with a predicted free-ion value of 0.85 μ_B. This is unlikely to be the case, as Weyl semimetals are almost always charge balanced. Introducing a Sm^{2+} cation introduces many unlikely scenarios to satisfy charge balance. It is more likely that our sample had degraded. In either case, the observed magnetism we do see in Sm_3HfBi_5 is likely due to bonds between the samarium atoms. Bonds which run along the length of the rod, down the c-axis, see Figure 3.11.

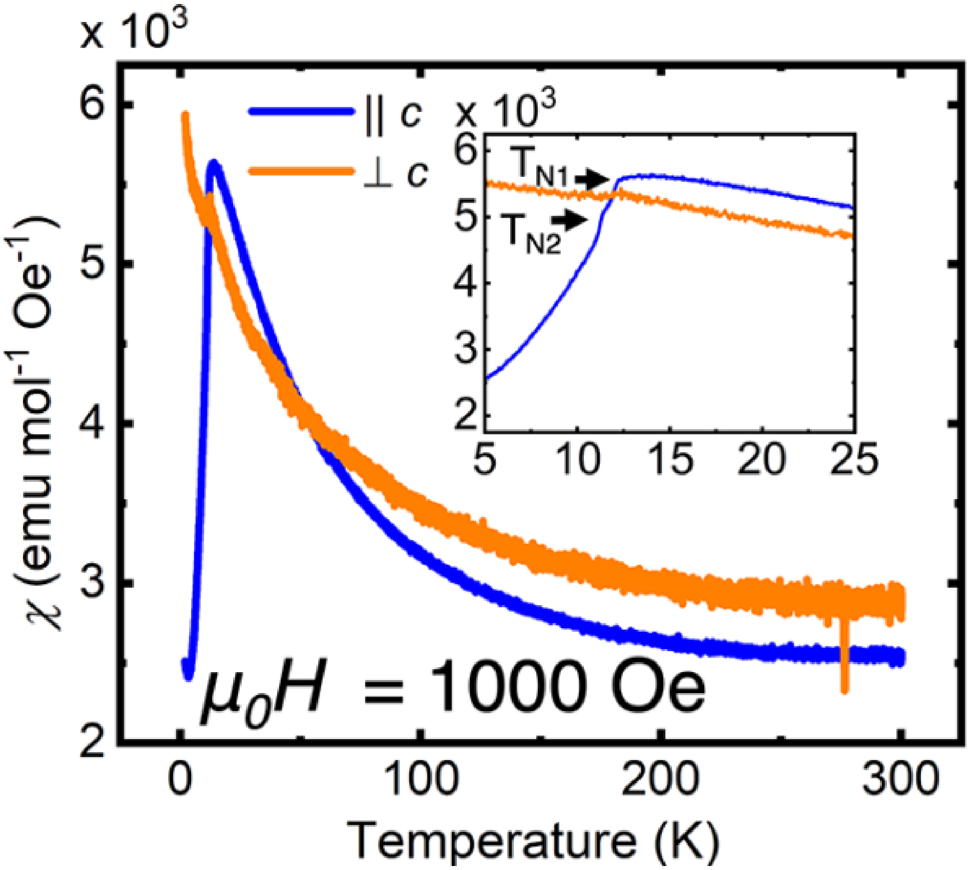

Figure 3.10. Magnetic susceptibility of Sm_3ZrBi_5 [15].

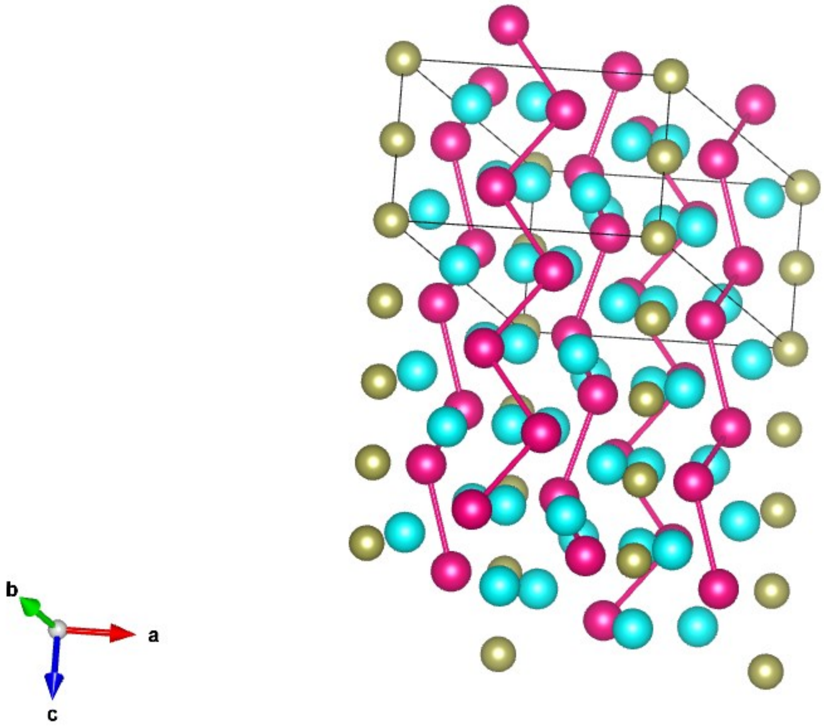

Figure 3.11. An image showing the Sm-Sm bonds running down the length of the Sm_3HfBi_5 rod.

When plotting the magnetism of Sm_3HfBi_5 against the externally applied magnetic field information about the low and high field saturations can be obtained. Figure 3.12 shows this plot for Sm_3HfBi_5. The significant change in slope in the middle is indicative of a low-field saturation. Often, materials will saturate at higher magnetic fields, yielding a flattened magnetism value under increasing magnetic fields. Sm_3HfBi_5 does not appear to saturate at the tested range of values. As stated above we observed a magnetic susceptibility value of ~0.03 μ_B /mol Sm. Such a value indicates the nonmagnetic variety of Sm^{2+} is present in the Sm_3HfBi_5 sample with some population of excited states contributing to overall magnetism.

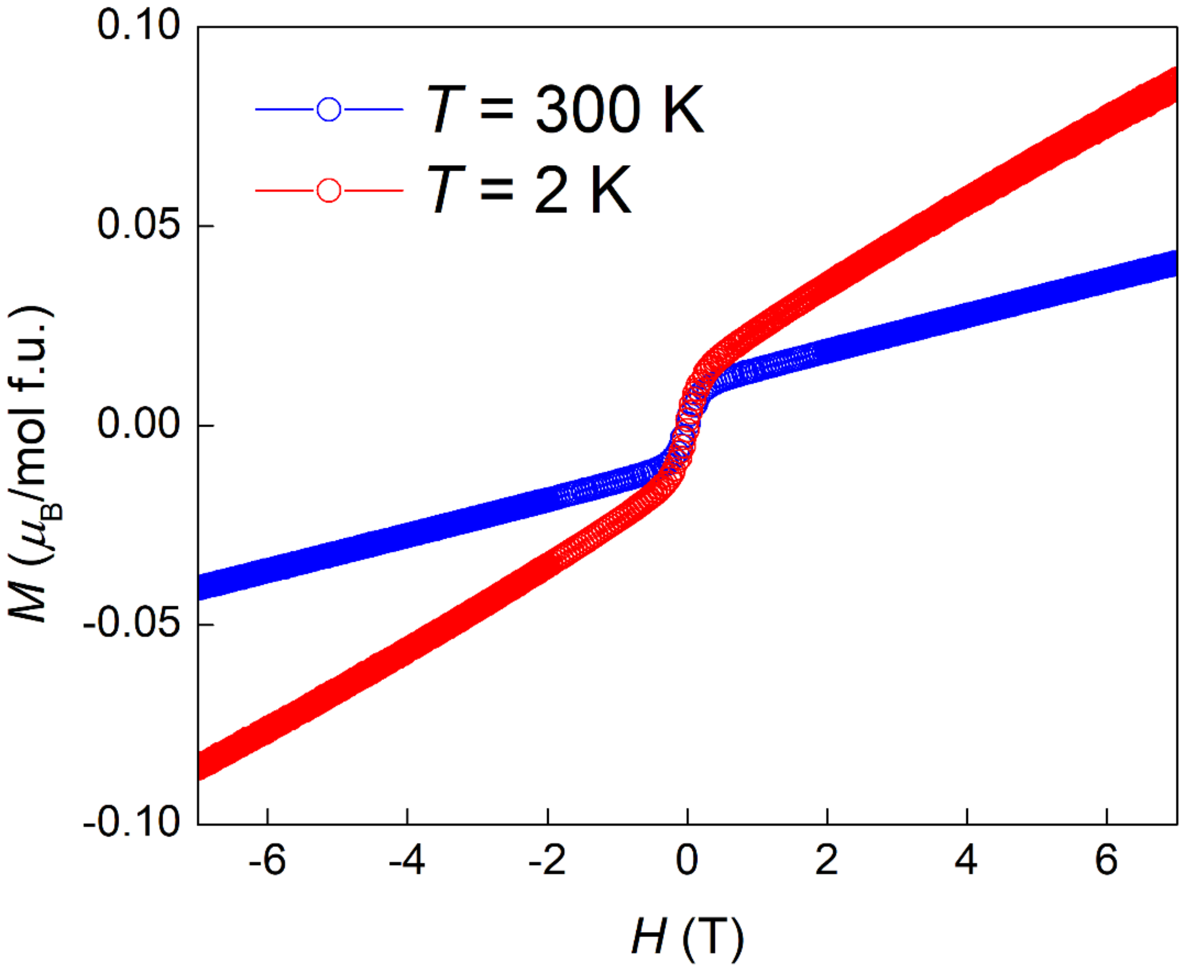

Figure 3.12. Magnetization compared to an external magnetic field for Sm_3HfBi_5.

CONCLUSION

Using flux growth methods, a single crystal of Sm_3HfBi_5, a potential Weyl semimetal, was grown in an evacuated ampoule with a vacuum down to roughly 3 milliTorr. The reactants were placed in a furnace and heated to 1000ºC then slowly cooled to 700ºC. After breaking open the reaction ampoules it was found that the crystals grew in hexagonal rods that are several millimeters in length and highly sensitive to air. Several samples were stored in a argon-atmosphere for months without degrading, but air sensitivity created difficulty when characterizing the material. The crystal structure was determined using single crystal x-ray diffraction and software designed to interpret such data. Powder x-ray diffraction was impossible due to rapid destruction of powdered Sm_3HfBi_5 in air, even when submerged in grease. Geometric models of the crystals were produced using VESTA software and a .cif file. Magnetic information about Sm_3HfBi_5, along the length of the rod, was obtained by sending the crystals to an outside lab for magnetization measurement. The magnetic and structural properties of Sm_3HfBi_5 were compared with several other similar materials in the same structural family.

REFERENCES

[1] B. Andrei Bernevig, *It's been a Weyl coming: Condensed-matter physics brings us quasiparticles that behave like massless fermions.*, Nat. Phys. **11**, 698-699 (2015).

[2] L. Schoop, X. Dai, R. J. Cava, and R. Ilan, *Special topic on topological semimetals-New Directions*, APL Mater. **8**, 030401 (2020).

[3] D. Ciudad, *Weyl fermions: massless but real*, Nat. Phys. **14**, 863 (2014).

[4] H. Weyl, *Electron and gravitation*, *z. Phys* **56**, 330-352 (1929).

[5] L. Schoop, F. Pielnhofer, and B. Lotsch, *Chemical Principles of Topological Semimetals*, Chem. Mater. **30**, 3155 (2018).

[6] Editorial, *After a Weyl*, Nat. Phys. **11**, 697 (2015).

[7] A. A. Burkov, *Toplogical semimetals*, Nat. Phys. **15**, 1145-1148 (2016).

[8] X. Wan, A. M. Turner, A. Vishwanath, and S. Y. Savrasov, *Topological semimetal and Fermi-arc surface states in the electronic structure of pyrochlore iridates*, Phys. Rev. B 83, 205101 – Published 2 May 2011

[9] S. Rao, *Weyl semi-metals: a short review*, arXiv: 1603.0282 (2016).

[10] B. Yan and C. Felser, *Topological Materials: Weyl Semimetals*, Annu. Rev. Condes. Matter Phys. **8**, 337-54 (2017).

[11] M. Koshino and I. F. Hizbullah, *Magnetic susceptibility in three-dimensional nodal semimetals*, Phys. Rev. **B 93**, 045201 (2016).

[12] J. R. Soh, P. Manuel, N. Schröter, F. Orlandi, Y. Shi, D. Prabhakaran, and A. Boothroyd, *Magnetic and electronic structure of Dirac semimetal candidate* $EuMnSb_2$, Phys. Rev. B **100**, 174406 (2019).

[13] R. Sultana, G. Gurjar, B Gahtori, S. Patnaik, and V. P. S. Awana, *Flux free single crystal growth and detailed physical property characterization of* $Bi_{1-x}Sb_x$ *(x = 0.05, 0.1 and 0.15) topological insulator*, Mat. Res. Exp., **6**, 106102 (2019).

[14] C. K. Aslani, V. V. Klepov, and H. zur Loye, *Flux Crystal Growth of a New* $BaTa_2O_6$ *Polymorph, and of the Novel Tantalum Oxyfluoride Salt Inclusion Phase* $Ba_3F]Ta_4O_{12}F$*: Flux Dependent Phase Formation*, Journal of Solid State Chemistry, **294**, 121833 (2020).

[15] J .F. Khoury, Bingzheng Han… and L. Schoop, *A Class of magnetic Topological material Candidates with Hypervalent Bi Chains*, J. Am. Chem. Soc., **144**, 9785-9796 (2022).

[16] J. F. Khoury, X. Song, and L. Schoop, *Ln_3MBi_5 (Ln =Pr, Nd, Sm; M=Zr, Hf): Intermetallics with Hypervalent Bismuth Chains*, Z. Anorg. Allg. Chem., **648**, e202200123, 1-8 (2022).

[17] J. Gibbs, *The Scientific Papers of J. Willard Gibbs, New Dover Edition. Vol. 1: Thermodynamics*, Dover Publications, Inc., Constable and Co., 1906 reprinted 1961.

[18] Crystallography matters ... more!, https://www.iycr2014.org/participate/crystal-growing-competition-2014/info-for-newcomers/how-to-grow.

[19] B. R. Pamplin, *Crystal growth* (Pergamon Press, Oxford, UK, (1975).

[20] S. Mugiraneza, A.M. Hallas, *Tutorial: a beginner's guide to interpreting magnetic susceptibility data with the Curie-Weiss law*, Comm. Phys, **5**, 95 (2022).

[21] T. Murakami, T. Yamamoto, F. Takeiri, K. Nakano, and H. Kageyama, *Hypervalent Bismuthides La3MBi5 (M = Ti, Zr, Hf) and Related Antimonides: Absence of Superconductivity*, Inorg. Chem., **56**, 5041−5045 (2017).

[22] S. H. D. Moore, L. Deakin, M. J. Ferguson, and A. Mar. *Physical Properties and Bonding in RE3TiSb5 (RE) La, Ce, Pr, Nd, Sm)*, Chem. Mater., **14**, 4867-4873 (2002).